ChemSusChem

Research Article
doi.org/10.1002/cssc.202200372

Chemistry Europe
European Chemical Societies Publishing

www.chemsuschem.org

Exploring the Interface of Porous Cathode/Bipolar Membrane for Mitigation of Inorganic Precipitates in Direct Seawater Electrolysis

Ji-Hyung Han*[a]

Direct seawater electrolysis utilizes natural seawater as the electrolyte. Hydroxide ions generated from the hydrogen evolution reaction at the cathode induce the precipitation of inorganic compounds, which block the active sites of the catalysts, leading to high cell voltage. To mitigate inorganic scaling, herein, an optimized interface between a porous electrode and a bipolar membrane (BPM, as a separator) was suggested in zero-gap seawater electrolyzers. Despite the formation of inorganic deposits at the front side (facing bulk seawater) of the porous cathode due to the water reduction reaction, the back side facing the cation exchange layer of the BPM remained free from thick inorganic deposits. This was ascribed to the locally acidic environment generated by proton flux from water dissociation at the BPM, enabling stable hydrogen production via the proton reduction at low overpotential. This asymmetric hydrogen evolution reaction at the porous cathode led to a considerably lower cell voltage and higher stability than that achieved with the mesh electrode. Moreover, precipitation at the front side of the porous cathode was further mitigated through acidification of the seawater by introducing an open area of the BPM that was not in contact with the porous cathode, allowing free protons that were not involved in the electron transfer reaction to diffuse out into the bulk seawater. These findings may provide critical guidance for the investigation of interfacial phenomena for the complete mitigation of inorganic scaling in the direct electrolytic splitting of seawater.

Introduction

Clean and renewable energy sources, such as solar and wind, are the key to achieving carbon neutrality, and hydrogen is an important energy carrier for managing the intermittency of renewable power generation.[1] In this trend, water electrolysis is an important process for producing green hydrogen from renewable sources using electricity.[2] When building industrial-scale electrolyzers in arid desert regions along ocean coastlines or on floating offshore wind platforms, the use of seawater, which accounts for 96.5% of the global water supply, as an unlimited electrolyte for water electrolysis, is prospectively sustainable. The first approach for utilizing seawater as a source of hydrogen is to remove all dissolved salts and produce ultra-purified water. The advantage of this approach is that it allows the use of highly mature technologies such as alkaline water electrolysis[3] and proton exchange membrane water electrolysis (PEMWE).[4] However, the production of high-purity water from seawater involves costly extensive water purification and desalination processes, as well as the associated investments for the plant, land, maintenance, and transportation.

The second approach, called direct seawater electrolysis (DSWE), directly uses seawater as an electrolyte, which can minimize capital expenditures associated with water sources. However, several fundamental and engineering challenges need to be addressed.[5,6] High concentration of chloride is one major concern. Corrosion due to chlorine gas and chloride ions limits the stability of the anode and cathode. For the anode, the chlorine evolution reaction [ClER; Eq. (1)] impedes the selective oxygen evolution reaction [OER; Eqs. (2) and (3)]:

$$2Cl^- \rightarrow Cl_2 + 2e^-;\ E^0 = 1.3583\ V \quad (1)$$

$$\text{acidic media}:\ 2H_2O \rightarrow O_2 + 4H^+ + 4e^-;\ E^0 = 1.229\ V \quad (2)$$

$$\text{basic media}:\ 4OH^- \rightarrow O_2 + 2H_2O + 4e^-;\ E^0 = 0.401\ V \quad (3)$$

The ClER, which involves the transfer of only two electrons, is kinetically much faster than the OER, which comprises four electron transfers and at least two or three intermediates.[7] It is critical to develop electrocatalysts with a high selectivity for OER at neutral pH as the average pH of seawater is near neutral, where Co-based catalysts exhibit improved OER performance.[8,9]

The formation of inorganic precipitates, such as magnesium hydroxide [$Mg(OH)_2$], is another persistent problem for cathode operation in seawater because the hydrogen evolution reaction (HER) driven by the electroreduction of water [Eq. (4)] in basic conditions abruptly increases the pH of the bulk catholyte.

[a] Dr. J.-H. Han
Jeju Global Research Centre
Korea Institute of Energy Research
200 Haemajihaean-ro, Gujwa-eup, Jeju 63357 (Republic of Korea)
E-mail: jihyung0760@kier.re.kr

Supporting information for this article is available on the WWW under https://doi.org/10.1002/cssc.202200372

$$2H_2O + 2e^- \rightarrow H_2 + 2OH^-;\ E^0 = -0.828\ V \quad (4)$$

The resulting deposits block the active sites of the catalysts, leading to high cell voltage. Lu et al. reported that inorganic scaling on the surface of the cathode decreased the current density by 50%.[10] The suspended precipitates in bulk electrolytes can also be detrimental to the flow of the feed solution in a stack during upscaling because the channels are easily clogged by fine particles. Despite the significance of inorganic fouling, few studies have suggested ways to mitigate the inorganic deposits. As merely temporary and expedient fixes, pure NaCl solutions,[11–14] strongly buffered seawater,[15–18] or alkalinized seawater[19] have been used.

Recently, Han et al. proposed a DSWE with a bipolar membrane (BPM) as a separator for controlling inorganic precipitates.[20] This is the first report of a combination of BPM and real seawater (as a catholyte) for hydrogen production. It was confirmed that seawater was acidified to pH 2 despite the significant generation of hydroxide ions in the HER. This acidification results from the cooperative effect of hydroxide ions trapped by inorganic precipitates at the mesh cathode and proton flux from water dissociation [WD; Eq. (5)] in the BPM.

$$H_2O \rightarrow H^+ + OH^- \quad (5)$$

The acidification of seawater reduces the overpotential for the HER and suppresses the formation of dispersed inorganic deposits. To stimulate the further development of BPM-based DSWE (BPM-DSWE) for the production of green hydrogen using seawater, mitigation of the formation of inorganic precipitates at the surface of the cathode and improving the performance and stability must be ensured.

This study presents a porous electrode/BPM interface in zero-gap direct seawater electrolyzers. The porous structure with a large surface area leads to a low specific current density (per real surface area), with low overpotential, enabling protons and hydroxide ions from WD to participate in the electron transfer reaction. It is confirmed that the back side of the porous cathode, in contact with the BPM, is locally acidified due to proton flux from the WD, preventing local precipitation of inorganic deposits in this area. In addition, it is demonstrated that open area of BPM, not in contact with a porous cathode and thereby exposed to the electrolyte, induces acidification of seawater, which further mitigates the formation of inorganic precipitates on the front side (facing bulk seawater) of the porous cathode. The approach used herein is applicable in electrochemical systems that utilize low-grade water (seawater or sewage effluent), where detrimental inorganic scaling occurs.

Experimental Section

Direct seawater electrolyzer

A batch-type cell, as described in a previous paper,[20] consisting of two chambers (acryl, internal dimension: $5\times5\times5\ cm^3$) with a BPM (Astom, Corp. Japan) as a separator, was used for electrolysis. Each chamber contained 120 mL of electrolyte. The effective area of the BPM ($7.065\ cm^2$) was identical to the geometrical area of the electrode. Two different electrodes were used: titanium fibers (Bekaert, Japan, diameter = 20 μm, weight = 400 g m^{-2}, porosity = 78%, thickness = 400 μm) and titanium mesh (Posco, Republic of Korea, 18 mesh, wire thickness = 230 μm, open area = 70%) coated with Pt or Ir; these electrodes are hereinafter called porous electrodes and mesh electrodes, respectively. The real surface area of the electrode was determined from the hydrogen adsorption/desorption peaks on Pt surfaces in cyclic voltammograms (scan rate, 50 $mV\,s^{-1}$, Supporting Information, Figure S1) with 1 M sulfuric acid solution using a conversion factor of 210 $\mu C\,cm^{-2}$.[21] The mesh and porous electrodes had roughness factors (ratio of the real surface area to the geometrical area) of 12 and 74, respectively. Additionally, visual observations of the changes in thickness and area of the white precipitates formed at the cathode interface over a 100 h period were made.

A zero-gap between the electrode and the BPM was applied to minimize bubble resistance. The electrolyzer was assembled by using a custom holder, which simultaneously applied pressure to the two chambers on both sides using a movable stainless-steel plate; natural seawater (37.0 $mS\,cm^{-1}$, pH 8.17), sea salt solution (38.0 $mS\,cm^{-1}$, pH 8.21), and 0.5 M NaCl (45.9 $mS\,cm^{-1}$, pH 7.2) were used as the catholyte. Without filtration or purification, natural seawater was used directly in the electrolyzer. NaOH (0.5 M) was used as the anolyte to achieve highly selective OER based on the greatest difference in the standard potentials of OER and ClER under alkaline conditions.[22] Because Na^+ is the predominant cationic component of natural seawater, NaOH was used as the anolyte rather than KOH to rule out the possibility of Na^+ crossover. It should be noted that chloride transport from the catholyte to the anolyte can be negligible in the BPM-DSWE; the concentration of chloride in the anolyte after 100 h of operation was confirmed to be around 300 ppm, which is slightly higher than the trace amount ($\approx$120 ppm) in the original NaOH solution (Figure S2).

Electrochemical characterization

Electrochemical tests were performed at room temperature (25 °C) using a potentiostat (ZIVE MP2 C, WonaTech, Republic of Korea). During the chronopotentiometric measurement of cell potential (E_{cell}) at $20\ mA\,cm^{-2}$ (normalized to the geometrical area of the electrode), cathode and anode potential (E_c and E_a) were monitored against an Ag/AgCl reference electrode using an auxiliary connection. The membrane potential (E_m) across the membrane was measured using two reference electrodes (Figure S3). To avoid a significant overpotential for WD in the BPM (Figure S4), a current density of $20\ mA\,cm^{-2}$ was chosen with an E_m of around 0.9 V, slightly greater than the thermodynamic potential for WD ($\approx$0.83 V). In addition, current–potential curves were recorded at a scan rate of $1\ mA\,s^{-1}$ with the same auxiliary connection. The gas produced in each chamber was collected in a gas bag (50 mL, Dalian Delin Gas Packing Co., Ltd., China) during the constant current test for a certain period. The bag was then connected to a gas chromatograph (GC 2014, Shimadzu, Japan) to evaluate the gas components and the amounts of hydrogen and oxygen.

Physical and chemical characterization

The porous cathodes with inorganic deposits were analyzed using field-emission scanning electron microscopy (FE-SEM; S-4800, Hitachi, Japan) coupled with quantitative energy-dispersive X-ray spectroscopy (EDS; XMAX 50, Horiba, Japan). The concentration of

chloride in the anolyte was determined using ion chromatography with an ICS-1600 instrument (Thermo Fisher Scientific).

Calculation of faradaic efficiency

The faradaic efficiency was calculated as the experimental moles of hydrogen or oxygen, divided by the theoretical value [Eqs. (6)–(8)].

$$\text{Faradaic efficiency} = \frac{\text{experimental moles}}{\text{theoretical moles}} \times 100 \quad (6)$$

$$\text{Experimental moles} = \frac{V}{V_0} \quad (7)$$

where V is the measured volume, V_0 is 24.45 L, and the gas volume is 1 mol at 1 atm and 298 K.

$$\text{Theoretical moles} = \frac{I \times t}{n \times F} \quad (8)$$

where I is the measured current, t is the time for gas collection, n is the stoichiometric number of electrons consumed in the electrode reaction ($n=2$ for hydrogen production, $n=4$ for oxygen production from WE), and F is the Faraday constant.

Results and Discussion

Although acidification of seawater in BPM-DSWE is very effective in suppressing the dispersed inorganic precipitates, as described in a previous report,[20] the inorganic deposits formed at the surface of the mesh-type cathode continue to grow over a long period of time (Figure 1). This indicates that the inorganic precipitation induced by hydroxide ions from the water reduction is faster than dissolution of the deposits in the acidified seawater. The acidified seawater is not effective for dissolving the thick inorganic precipitates, unlike a high concentration of acid solution. Therefore, a strategy is needed to retard the growth of inorganic precipitates at the surface of the cathode.

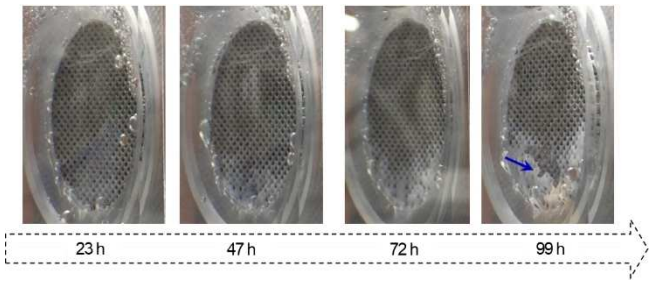

Figure 1. Photographs of Pt mesh cathode in natural seawater as a catholyte under constant geometrical current density (20 mA cm^{-2}). Hydrogen is constantly being produced. Thick and bulky inorganic precipitates grow at the lower part of the cathode surface during long-term operation. Around 99 h, the bulky deposit (indicated as a blue arrow) is separated from the surface of the cathode due to acidified seawater and new inorganic precipitate grows slowly on that surface.

To minimize the growth of bulky inorganic deposits on the surface of the cathode, a porous electrode was used (Figure S5). Titanium fibers, typically used as the porous transport layer in PEMWE and fuel cells,[23,24] were utilized as substrates. Despite the high probability that small pores will be clogged by the inorganic precipitates, the porous structure provides a large surface area, enabling a lower specific current density (normalized to the real surface area of the electrode) than that of the mesh structure under constant current operation. Therefore, it is expected that the inorganic deposits formed at the porous electrode under a low specific current density will be much thinner than those formed on the mesh electrode.

First, focus was placed on the large difference in E_{cell} before describing the precipitation of inorganics at the porous electrodes in BPM-DSWE (Figure 2a). The E_{cell} of the porous Pt electrode was much lower ($\approx$1.1 V at 100 h) than that of the mesh electrode. During the measurement of E_{cell}, E_c, E_a, and E_m were monitored using Ag/AgCl reference electrodes. The large decrease in E_{cell} originates from E_c and E_a; the differences in E_c and E_a between the two electrodes at approximately 100 h were 228 and 924 mV, respectively (Figure 2b,c). The difference in E_m was not large enough to affect E_{cell} (Figure S6). The significant decrease in the electrode potential for the HER and OER when porous electrodes are used indicates that electron transfer reactions are likely to involve not only water molecules, but also protons and hydroxide ions generated by WD in the BPM (as discussed hereinafter). The porous electrode is also much more stable than the mesh electrode, with E_{cell} degradation rates of 0.3 and 3.55 mV h^{-1} for the porous and mesh electrodes, respectively. This implies that none of the pores in the porous electrode becomes clogged with the inorganic precipitates during long-term operation. Notably, the current-potential curve does not reflect the cathode potentials measured in the long-term operation of BPM-DSWE (Figure S7).

Two kinds of electrocatalysts, Pt and Ir, were used for the electrodes, and the EDS data are shown in Figure S8. Ir shows better electrocatalytic ability for the OER, as is well known;[25] for the porous Ir anode, E_a was less positive than for the porous Pt anode (Figure S9a). In contrast, for the HER, both Pt and Ir showed similar E_c values (Figure S9b). Notably, the pH variation of seawater and the inorganic precipitation (discussed in the following sections) were not affected by the type of catalyst.

Interestingly, the pH of the bulk catholyte changed significantly depending on the electrode structure (Figure 3a). With the mesh cathode, the pH of the seawater was lowered to 3 in 2 h, as described in a previous paper,[20] whereas with the porous electrode, the initial pH (pH$\approx$8.5) of the seawater was maintained. In contrast, 0.5 M NaCl solution underwent rapid alkalization (pH$\approx$10) in 2 h, which definitively confirms the precipitation of inorganics at the porous cathode in seawater; this process captures the hydroxide ions generated by the electroreduction of water, suppressing the pH rise. The organic substances in natural seawater have a negligible effect on the pH of the bulk catholyte because there is no difference in the pH of natural seawater versus sea salt solution (Figure S10). Despite the high electrical resistance of the cathode surface due to the formation of inorganic deposits, the E_c obtained

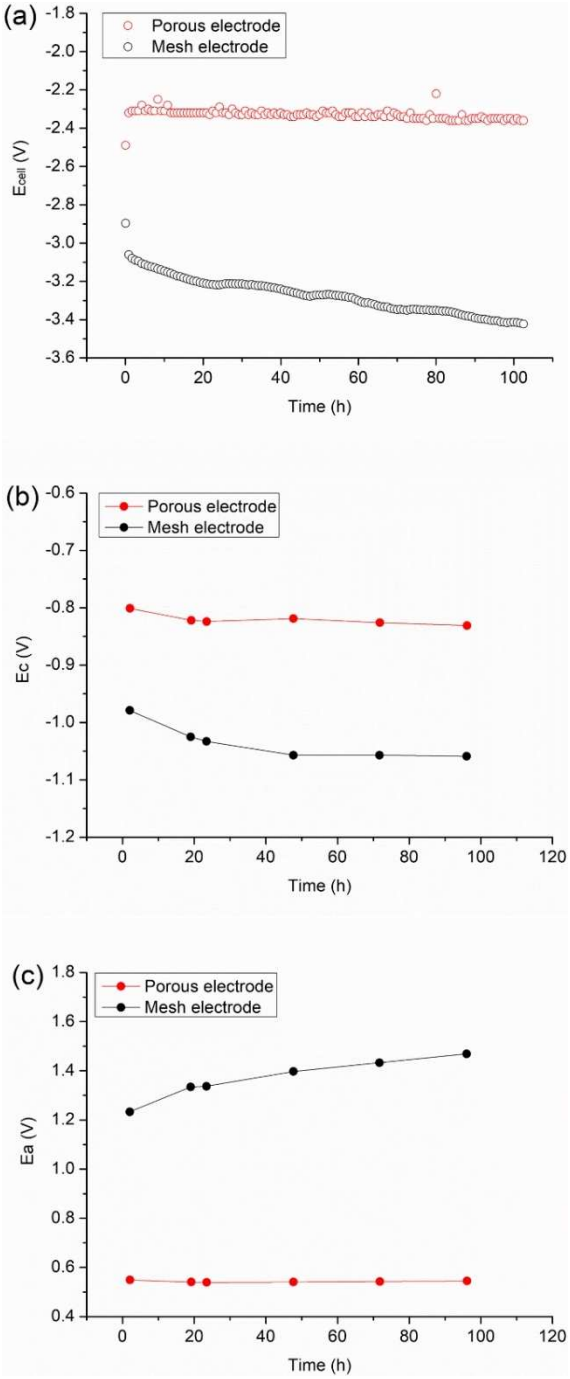

Figure 2. Shift of (a) cell potential (E_{cell}), (b) cathode potential (E_c), and (c) anode potential (E_a) with two different Pt electrodes (mesh or porous) at constant geometrical current density (20 mA cm^{-2}). Catholyte and anolyte are natural seawater and 0.5 M NaOH, respectively.

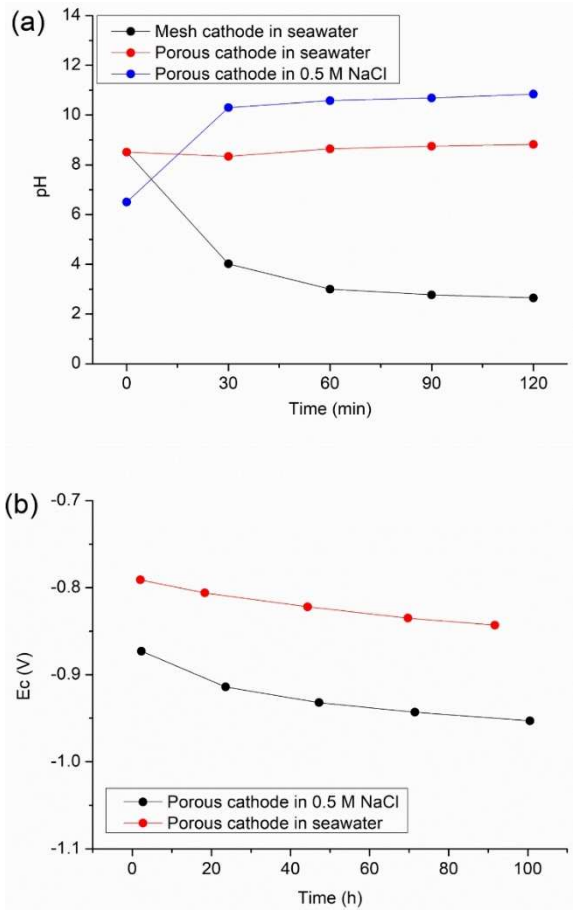

Figure 3. (a) Variation in pH of bulk catholyte over time with two different cathodes (mesh and porous) and two different catholytes (0.5 M NaCl and natural seawater). (b) Shift of E_c for porous cathode with two different catholytes over 100 h. Geometrical current density was 20 mA cm^{-2}.

with seawater at constant a pH of 10.2 over 100 h was less negative than that obtained with strongly alkaline (pH ≈ 12.5) 0.5 M NaCl solution (Figure 3b); the difference in E_c between the two electrodes was constant at approximately 88 mV. This is based on the Nernstian relationship,[26,27] where the equilibrium potential (E_{eq}) for the HER shifts negatively as the pH increases [Eq. (9)]:

$$E_{eq} = -0.059 \times \text{pH} \quad (9)$$

Meanwhile, regardless of the electrode structure, the anolyte maintained a strong alkalinity (pH ≈ 13) (Figure S11).

To explain the effect of the electrode structure on the large difference in the bulk pH of seawater, the aforementioned changes in E_c and E_a were considered. The electrode potential for the HER and OER decreased significantly with the porous electrode structure. The mesh cathode has a low surface area, leading to a high specific current density. With an increase in the overpotential for the HER to achieve a high current density, electroreduction of water becomes dominant (Figure 4a). The inorganic precipitation at the cathode surface captures the hydroxide ions produced from water reduction, suppressing the pH increase and growing the inorganic deposits. At the same time, protons from WD in the BPM acidify the seawater and dissolve part of the deposits at the cathode surface. Oxygen evolution, similar to the HER, is mainly achieved by the oxidation of water due to the high overpotential of this reaction. Protons generated from water oxidation are compensated by hydroxide ions from the WD in the BPM, maintaining strong alkalinity (pH ≈ 13).

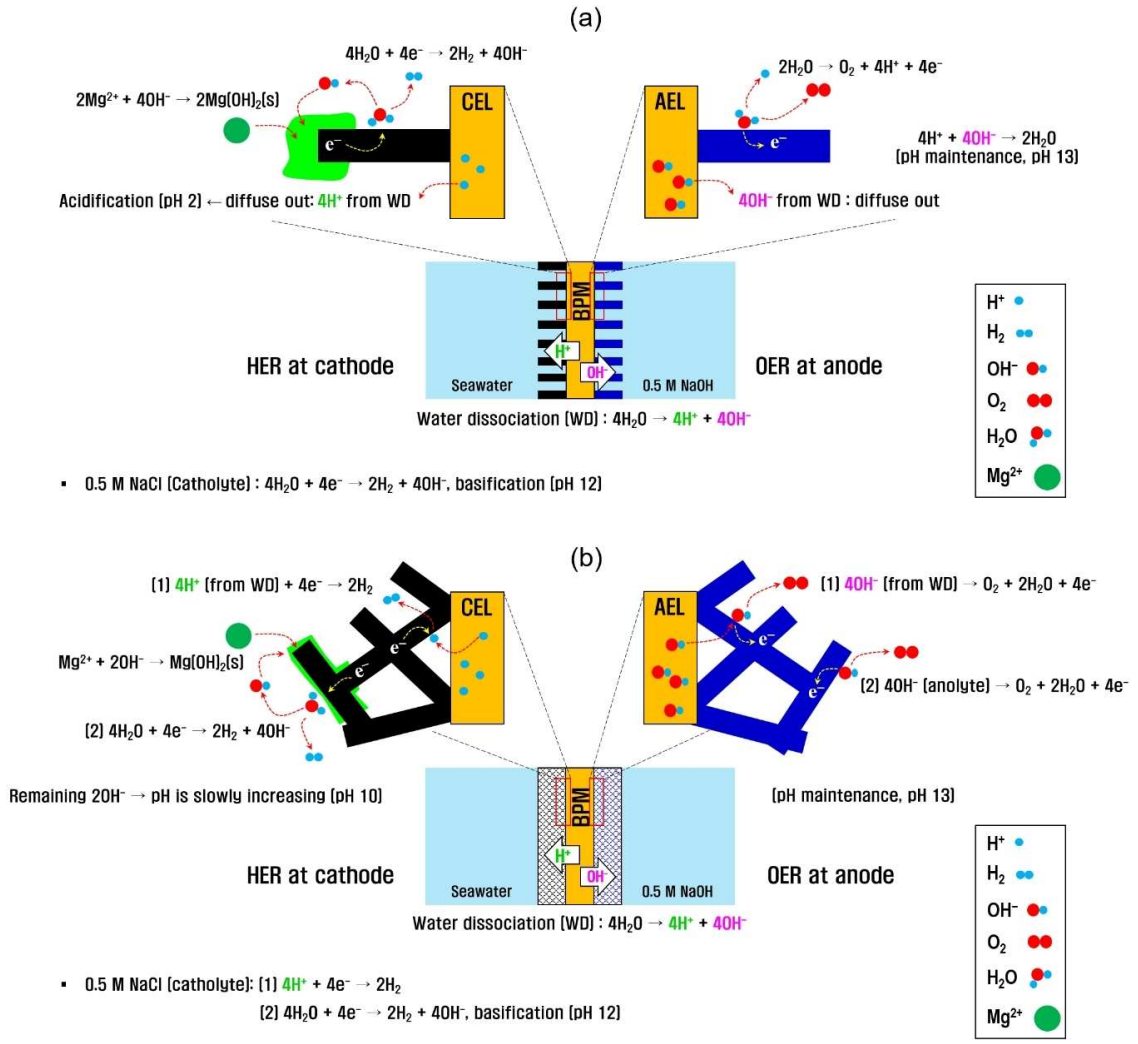

Figure 4. (a) Mesh cathode with small surface area: seawater is acidified by cooperative effect between electroreduction of water, inorganic precipitation capturing hydroxide ions, and proton flux from WD in BPM. (b) Porous cathode with large surface area: seawater is not acidified by proton reduction reaction and inorganic precipitation under low specific current density. The asymmetric HER proceeds via water reduction and proton reduction at the front (facing the catholyte) and back [facing the cation exchange layer (CEL) of the BPM] sides, respectively, of the porous cathode. The electrochemical equations provide quantitative information for understanding the effect of the electrode structure on the pH variation, inorganic precipitation, HER, and OER in BPM-DSWE. AEL: anion exchange layer.

In contrast, the porous electrodes generally provide a large surface area, which leads to a low specific current density and a corresponding low activation overpotential.[28] Under these circumstances, protons and hydroxide ions from WD in the BPM play an important role in the charge-transfer reaction. The confinement effect[29,30] of the porous structure also increases reactant's stay near the electrode surface, which enables protons and hydroxide ions generated from the WD to undergo electron transfer. Most importantly, since seawater is acidified only when the protons produced by the WD of BPM diffuse into the bulk catholyte, the basification of seawater observed indicates that the proton reduction reaction actually occurs. Therefore, at the porous cathode, both water molecules and protons undergo electrochemical reduction to produce hydrogen (Figure 4b). Because protons as a source of seawater acidification participate in electron transfer, seawater is not acidified and the pH of the bulk seawater slowly increases with time; the initial pH increases to 10.28 in 24 h, which is maintained for 100 h. This can be attributed to a small portion of free hydroxide ions, which are not fixed in inorganic precipitates.

The 0.5 M NaCl solution with the porous cathode undergoes rapid alkalization, reaching pH 10.8 in 2 h and pH 12.5 at 100 h. This is because the water reduction reaction produces hydroxide ions, and the hydrogen evolution reaction consumes the protons generated by the WD. In the case of the porous anode that shows a much larger decrease in the electrode potential for the OER, hydroxide ions generated from WD are expected to be the main reactants. When pure water is used as an anolyte, the pH of the anolyte is reduced to 3. (Figure S12a). This means that water molecules undergo oxidation to produce protons, despite the fact that WD supplies the anolyte with

hydroxide ions. As a result, hydroxide ions in NaOH solution are expected to participate in the electron transfer reaction as well. It should be noted that water molecules generated during the electrooxidation of hydroxide ions are re-consumed in the BPM via WD, thereby maintaining a high degree of alkalinity.

As mentioned above, the pH of the seawater at the porous cathode slowly increased to 10 over the course of 100 h. The bulk seawater remained transparent for 24 h, after which inorganic precipitates began to accumulate at the bottom of the electrolyzer (indicated by blue arrows in Figure 5). However, it is interesting that E_c was quite constant (Figure 2b), although the surface of the cathode was covered with thin inorganic precipitates. It is thought that the HER is maintained through the proton reduction reaction on the back side facing the cation exchange layer (CEL) of the BPM, which is locally acidic due to proton flux from WD. This was confirmed by the absence of hydrogen bubbles at the front side (facing the catholyte) of the cathode. Most of the bubbles (indicated by red arrows in Figure 5 and Supporting Information video) only emerged from the top of the cathode at a high flux rate. Therefore, the asymmetric HER at the porous cathode was expected to occur as follows (Figure 4b).

Back side: proton reduction reaction [Eq. (10)].

$$4H^{+}(\text{from WD}) + 4e^{-} \rightarrow 2H_{2(g)} \quad (10)$$

Front side: water reduction reaction [Eq. (11)]; inorganic precipitation [Eq. (12)], forming thin deposits under low current density; and diffusion of $2OH^{-}$ into the bulk catholyte (seawater basification, pH 10).

$$4H_2O + 4e^{-} \rightarrow 2H_2 + 4OH^{-} \quad (11)$$

$$Mg^{2+} + 2OH^{-} \rightarrow Mg(OH)_{2(s)} \quad (12)$$

This asymmetric HER at the porous cathode/BPM interface was reconfirmed by the obvious difference in the amount of inorganic deposits at the front versus the back side of the porous cathode (Figure 6a,b), where the front side was covered with white deposits, whereas there were no visible deposits on the back side. The fibers on the front side were completely covered with thick plate-shaped inorganic deposits (Figure 6c), with an atomic percentage of Mg of approximately 24% (full EDS data are shown in Figure S13). In contrast, the fibers in direct contact with the CEL of the BPM were covered with very thin deposits (Figure 6d-1) having a low atomic percentage ($\approx$3%) of Mg. The fibers located immediately below were covered with a considerably thick layer of inorganic precipitates (Figure 6d-2), although these deposits were thinner than the fibers on the front side.

Considerably thinner inorganic precipitates were formed on the porous electrode than the mesh electrode on which the deposits were thick enough to reduce the effective area of the BPM (Figure S14). However, there is still a high probability of pore clogging during operation for more than 100 h. In addition, deposits at the bottom of the electrolyzer can become stuck in the channels of the flow-type stack. Therefore, another strategy for suppressing the pH increase is needed to further mitigate inorganic scaling. To achieve this objective, herein, an open area of the porous cathode was created by cutting out a part of the electrode; this open area allows protons from WD to diffuse out into the bulk seawater without undergoing the proton reduction reaction. These free protons contribute to the acidification of seawater (Figure 7a).

Figure 7b shows the significant effect of the open area of the electrode on the pH of bulk seawater. The wider the open area, the faster the rate of acidification of the seawater (Figure 7b). With an open area corresponding to 2.2% of the geometrical area of the porous cathode, the pH of the bulk seawater slowly decreased to 3.9 in 100 h. With an open area of 4%, the pH reached 3 in 24 h, and with an open area of 11.3%, a much faster decrease in the pH (pH 3 in 2 h) was achieved. The acidification rate was directly reflected in E_c (Figure 7c). When the porous cathodes with a fast acidification rate (open area of 4 and 11.3%) were used, E_c decreased within 24 h. In contrast, with an open area of 0 or 2.2% where pH remained basic or decreased slowly, E_c increased slowly in the negative direction without ever decreasing. The decrease in the real surface area due to the open area can have a negative effect on E_c depending on the size of the open area; an open area of 22.6% leads to a large increase in E_c ($\approx$100 mV). This indicates that a minimum open area is required to provide a large

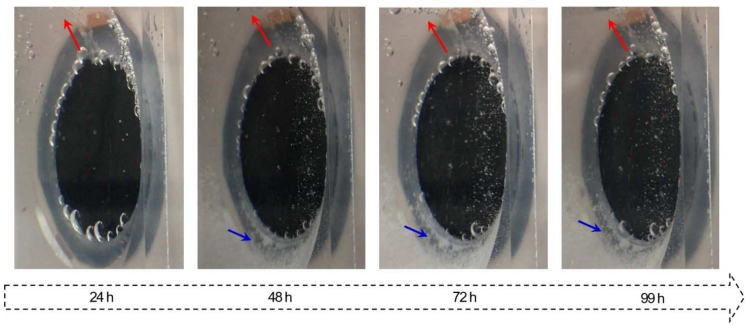

Figure 5. Photographs of porous cathode in natural seawater as a catholyte under constant geometrical current density (20 mA cm^{-2}). Inorganic precipitates (indicated by blue arrows) accumulate at the bottom of the electrolyzer after 24 h, and hydrogen bubbles are only emerging from the top of the cathode (indicated by red arrows).

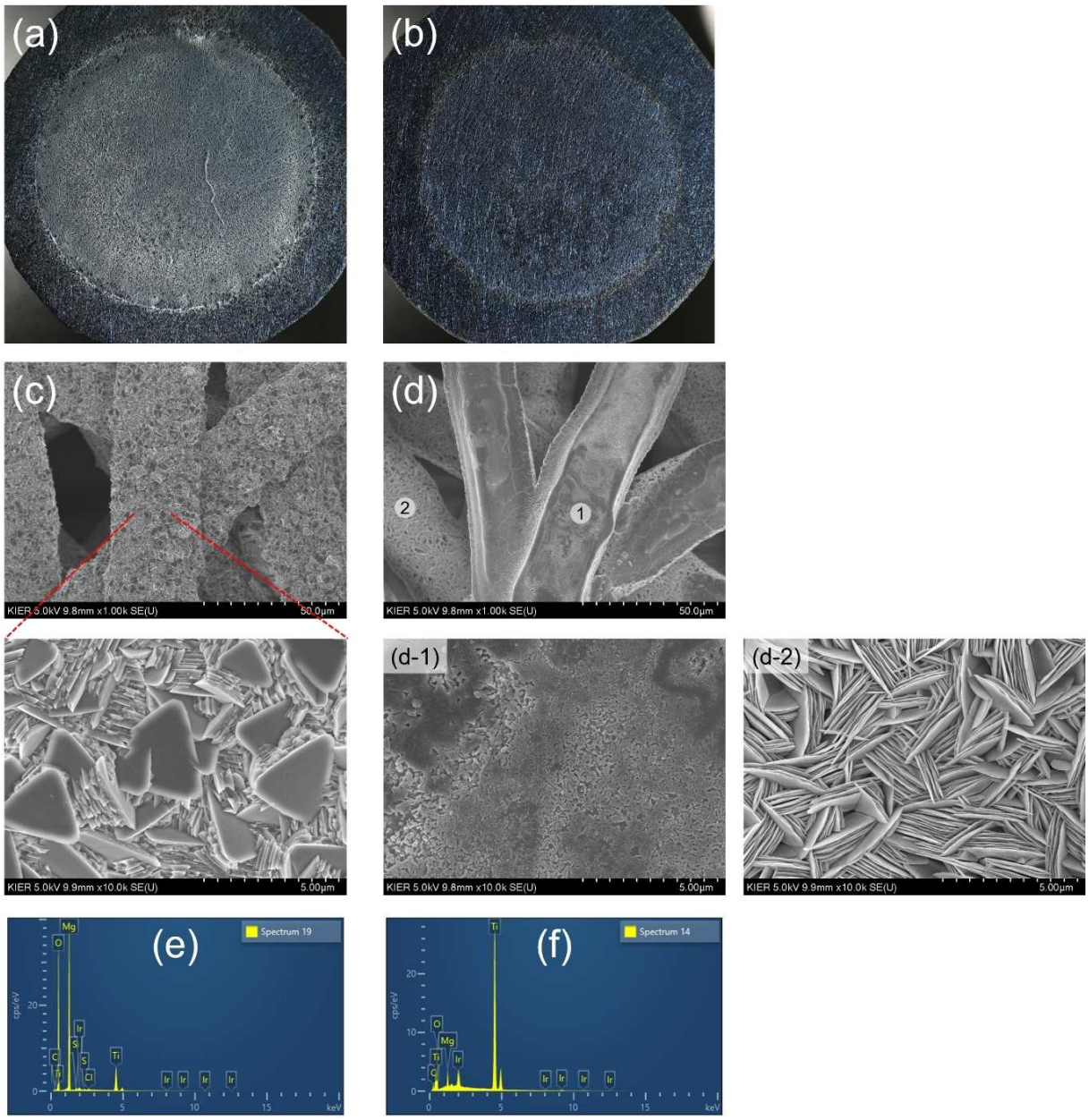

Figure 6. Photographs of (a) front (facing the catholyte) and (b) back (facing the CEL of the BPM) sides of porous cathode after operation at geometrical current density of 20 mA cm^{-2} for 100 h. SEM images of (c) front and (d) back sides. EDS data for (e) front and (f) back sides.

enough surface area for inducing the proton reduction reaction and to suppress the pH increase of the bulk seawater.

The open area of the porous cathode had a negligible effect on E_m (Figure S15a). E_a was also nearly identical with a small deviation (≈30 mV), owing to the use of porous Ir anodes in all cases. As a result, the change in E_{cell} reflects the change in E_c in its current state (Figure S15b). Rapid acidification rates of 4 and 11.3% resulted in a significant decrease in E_{cell} after 24 h. The open area of 4% with the lowest E_c value around 100 h corresponds to the lowest E_{cell} value. As shown in E_c, the open area of 22.6% exhibited the greatest increase in E_{cell}.

Seawater acidification by the open area not only eliminated the accumulation of inorganic debris at the bottom of the electrolyzer (Figure S16), but also mitigated the formation of inorganic precipitates at the front side of the porous cathode. Figure 8a shows the absence of noticeable white deposits on the front side of the porous cathode with an open area of 4%. It was confirmed that a very small amount of inorganic precipitates was formed (Figure 8a-1) with a low atomic percentage (1–2%) of Mg (Figure S17). In contrast, the pores in the outer part of the effective area of the BPM, which is not directly in contact with the acidified seawater, were completely clogged with thick inorganic deposits (Figure 8a-2).

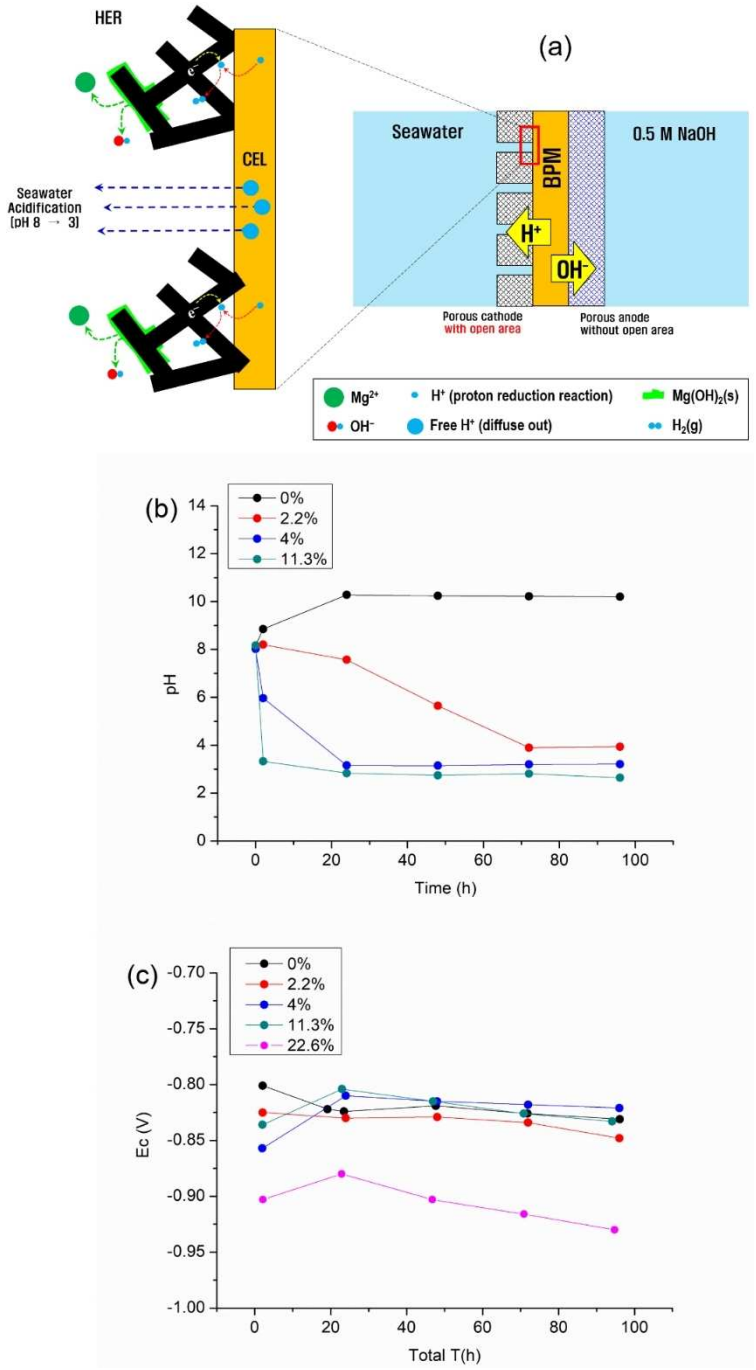

Figure 7. (a) Seawater acidification by free protons (blue large circles) diffusing out through open area of porous cathode. (b) Variation in pH of bulk seawater and (c) shift of E_c according to different percentages of open area of porous cathode. Constant geometrical current density (20 mA cm^{-2}) was applied over 100 h. Catholyte and anolyte are natural seawater and 0.5 M NaOH, respectively.

The most notable aspect on the back side of the porous cathode is, as shown in Figure 8b-2, the absence of thick deposits on not only the fibers closest to the CEL of the BPM, but also on the inner fibers, unlike in the absence of the open area (Figure 6d-2). This indicates that seawater acidification completely suppresses the formation of thick precipitates on both sides of the porous cathode, especially at the edges. In contrast, some deposits were formed in the center (Figure 8b), which was covered with round plate-shaped inorganic precipitates (Figure 8b-1). White deposits were radially formed inside the porous cathode with an open area of 2% (Figure S18a). For the porous cathode with a rectangular-shaped open area of 11%, no deposit was formed around the open area, but radial inorganic deposits were formed inside (Figure S18b). The radial pattern and the degree of precipitates are expected to vary depending on the location and size of the open area, which

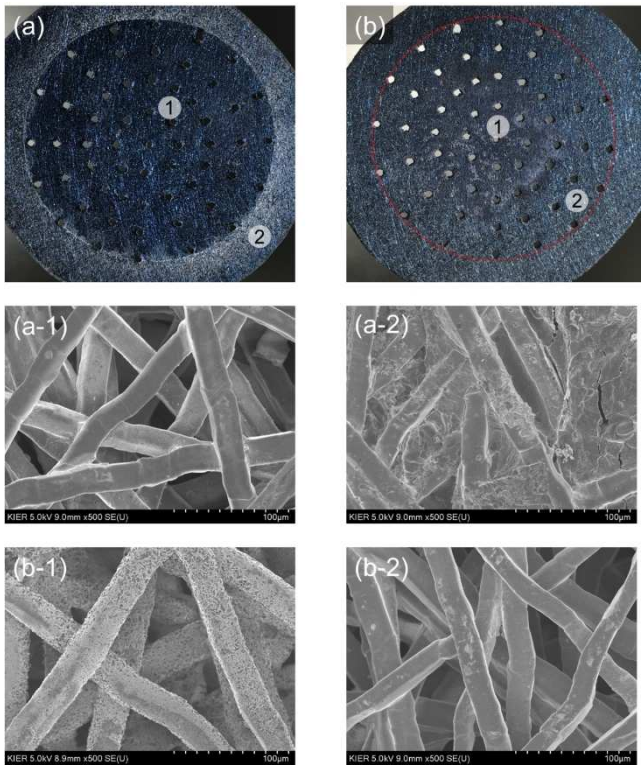

Figure 8. Photographs of (a) front and (b) back sides of porous cathode with an open area of 4% after 100 h of operation. Red dotted line indicates the boundary of the effective area of the BPM. SEM images of front (a-1, a-2) and back (b-1, b-2) sides. EDS data for each part are shown in Figure S17. Scale bars for a-1, a-2, b-1, and b-2: 100 μm.

seem to affect the competitive reaction between the water reduction reaction and proton reduction reaction. The formation of hydrogen bubbles can also possibly prevent contact with the acidified seawater, causing inorganic deposits to grow.

In comparison to mesh electrodes, the H_2 faradaic efficiency of the porous cathode was low (≈75%), despite the fact that the purity of hydrogen was around 99% (Figure S19). This is because the volume of hydrogen collected fell short of the theoretical value. The trapped hydrogen bubbles in the narrow spaces of the porous cathode are expected to be the primary cause. It was confirmed that large hydrogen bubbles were generated primarily from the open area of the cathode rather than small bubbles on the front side of the cathode. This indicates that the small bubbles generated on the back side of the porous cathode coalesce into the large bubbles. the confined spaces of the porous cathode are expected to impede the growth and diffusion of the hydrogen bubbles. Additionally, the interfacial property (hydrophobicity or hydrophilicity) of the porous cathode can change as the seawater electrolysis proceeds, causing the amount of hydrogen collected to vary over time. This is the point at which the surface of the porous cathode must be modified to transport hydrogen bubbles effectively and release them into the bulk catholyte.[24] Therefore, the optimized open area (i.e., size and location) and surface modification of the porous cathode are expected to minimize inorganic deposits and maximize Faradaic efficiency for H_2, enabling the DSWE to operate at a high level of performance and stability. This requires a more in-depth examination.

Conclusions

This study, focusing on the mitigation of inorganic precipitation, demonstrates the significant impact of optimizing the porous electrode/bipolar membrane (BPM) interface on the performance and stability of direct seawater electrolysis (DSWE). A porous structure with a large surface area decreases the overpotential for the hydrogen (HER) and oxygen evolution reactions (OER), enabling protons and hydroxide ions generated from water dissociation (WD) in the BPM to participate in the electron transfer reaction. The back side (facing the BPM) of the porous cathode, where the proton reduction reaction mainly occurs, is free from thick inorganic deposits, improving the reaction stability. Coverage of the front side (facing the catholyte) of the porous cathode by thick inorganic deposits from the electroreduction of water is further mitigated by suppressing the increase in the pH of bulk seawater. This is achieved by introducing a small open area of the BPM that does not come into contact with the porous cathode; protons from WD in the BPM freely diffuse out of the open area into the electrolyte, thereby acidifying the seawater. These interfacial phenomena in the porous cathode/BPM with natural seawater as a catholyte are applicable to low-grade water-related electrochemical systems such as reverse electrodialysis, microbial electrolysis, and photoelectrochemical seawater splitting, and minimize severe inorganic scaling, opening up new possibilities for the development of stack systems for seawater electrolyzers.

Acknowledgements

This work was conducted under the National Research Foundation of Korea (NRF) grant funded by the Korean Government (MSIT) (No. 2019R1 C1 C1002847) and the framework of the research and development program of the Korea Institute of Energy Research (KIER) (C1-2457). I would like to thank Mr. Sung Don Kim for his help with the seawater collection.

Conflict of Interest

The authors declare no conflict of interest.

Data Availability Statement

The data that support the findings of this study are available from the corresponding author upon reasonable request.

Keywords: direct seawater electrolysis · inorganic precipitation · bipolar membrane · renewable hydrogen · water splitting

[1] A. Saeedmanesh, M. A. Mac Kinnon, J. Brouwer, *Curr. Opin. Electrochem.* **2018**, *12*, 166–181.
[2] G. Glenk, S. Reichelstein, *Nat. Energy* **2019**, *4*, 216–222.
[3] K. Zeng, D. Zhang, *Prog. Energy Combust. Sci.* **2010**, *36*, 307–326.
[4] L. Ma, S. Sui, Y. Zhai, *Int. J. Hydrogen Energy* **2009**, *34*, 678–684.
[5] W. Tong, M. Forster, F. Dionigi, S. Dresp, R. Sadeghi Erami, P. Strasser, A. J. Cowan, P. Farràs, *Nat. Energy* **2020**, *5*, 367–377.
[6] S. Dresp, F. Dionigi, M. Klingenhof, P. Strasser, *ACS Energy Lett.* **2019**, *4*, 933–942.
[7] J. G. Vos, T. A. Wezendonk, A. W. Jeremiasse, M. T. M. Koper, *J. Am. Chem. Soc.* **2018**, *140*, 10270–10281.
[8] Y. Surendranath, M. Dincă, D. G. Nocera, *J. Am. Chem. Soc.* **2009**, *131*, 2615–2620.
[9] F. Cheng, X. Feng, X. Chen, W. Lin, J. Rong, W. Yang, *Electrochim. Acta* **2017**, *251*, 336–343.
[10] X. Lu, J. Pan, E. Lovell, T. H. Tan, Y. H. Ng, R. Amal, *Energy Environ. Sci.* **2018**, *11*, 1898–1910.
[11] S. Dresp, T. Ngo Thanh, M. Klingenhof, S. Brückner, P. Hauke, P. Strasser, *Energy Environ. Sci.* **2020**, *13*, 1725–1729.
[12] S. Dresp, F. Dionigi, S. Loos, J. Ferreira de Araujo, C. Spöri, M. Gliech, H. Dau, P. Strasser, *Adv. Energy Mater.* **2018**, *8*, 1800338.
[13] B. C. M. Martindale, E. Reisner, *Adv. Energy Mater.* **2016**, *6*, 1502095.
[14] L. J. Song, H. M. Meng, *Int. J. Hydrogen Energy* **2010**, *35*, 10060–10066.
[15] S. Gao, G.-D. Li, Y. Liu, H. Chen, L.-L. Feng, Y. Wang, M. Yang, D. Wang, S. Wang, X. Zou, *Nanoscale* **2015**, *7*, 2306–2316.
[16] S.-H. Hsu, J. Miao, L. Zhang, J. Gao, H. Wang, H. Tao, S.-F. Hung, A. Vasileff, S. Z. Qiao, B. Liu, *Adv. Mater.* **2018**, *30*, 1707261.
[17] Y. Zhao, B. Jin, Y. Zheng, H. Jin, Y. Jiao, S.-Z. Qiao, *Adv. Energy Mater.* **2018**, *8*, 1801926.
[18] Y. Zhao, B. Jin, A. Vasileff, Y. Jiao, S.-Z. Qiao, *J. Mater. Chem. A* **2019**, *7*, 8117–8121.
[19] Y. Kuang, M. J. Kenney, Y. Meng, W.-H. Hung, Y. Liu, J. E. Huang, R. Prasanna, P. Li, Y. Li, L. Wang, M.-C. Lin, M. D. McGehee, X. Sun, H. Dai, *Proc. Natl. Acad. Sci. USA* **2019**, *116*, 6624–6629.
[20] J.-H. Han, E. Jwa, H. Lee, E. J. Kim, J.-Y. Nam, K. S. Hwang, N. Jeong, J. Choi, H. Kim, Y.-C. Jeung, T. D. Chung, *Chem. Eng. J.* **2022**, *429*, 132383.
[21] S. Trasatti, O. A. Petrii, *J. Electroanal. Chem.* **1992**, *327*, 353–376.
[22] F. Dionigi, T. Reier, Z. Pawolek, M. Gliech, P. Strasser, *ChemSusChem* **2016**, *9*, 962–972.
[23] C. Liu, M. Shviro, A. S. Gago, S. F. Zaccarine, G. Bender, P. Gazdzicki, T. Morawietz, I. Biswas, M. Rasinski, A. Everwand, R. Schierholz, J. Pfeilsticker, M. Müller, P. P. Lopes, R.-A. Eichel, B. Pivovar, S. Pylypenko, K. A. Friedrich, W. Lehnert, M. Carmo, *Adv. Energy Mater.* **2021**, *11*, 2002926.
[24] A. Lim, H.-Y. Jeong, Y. Lim, J. Y. Kim, H. Y. Park, J. H. Jang, Y.-E. Sung, J. M. Kim, H. S. Park, *Sci. Adv.* **2021**, *7*, eabf7866.
[25] C. C. L. McCrory, S. Jung, J. C. Peters, T. F. Jaramillo, *J. Am. Chem. Soc.* **2013**, *135*, 16977–16987.
[26] T. Shinagawa, K. Takanabe, *ChemSusChem* **2017**, *10*, 1318–1336.
[27] J. E. Bennett, *Int. J. Hydrogen Energy* **1980**, *5*, 401–408.
[28] A. J. Bard, L. R. Faulkner, *Electrochemical Methods: Fundamentals and Applications*, 2nd Edition, Wiley, **2000**.
[29] J.-H. Han, J. H. Bae, D. Han, T. D. Chung, *Electrochim. Acta* **2016**, *187*, 457–464.
[30] J.-H. Han, E. Lee, S. Park, R. Chang, T. D. Chung, *J. Phys. Chem. C* **2010**, *114*, 9546–9553.

Manuscript received: February 20, 2022
Revised manuscript received: March 23, 2022
Accepted manuscript online: March 24, 2022
Version of record online: April 27, 2022